Journal of Alloys and Compounds 695 (2017) 3704–3713

Contents lists available at ScienceDirect

Journal of Alloys and Compounds

journal homepage: http://www.elsevier.com/locate/jalcom

Synthesis and properties of $Bi_5Nb_3O_{15}$ thin films prepared by dual co-sputtering

Osmary Depablos-Rivera [a, b], Juan C. Medina [a, b, *], Monserrat Bizarro [a], Ana Martínez [a], Andreas Zeinert [c], Sandra E. Rodil [a]

[a] Instituto de Investigaciones en Materiales, UNAM, Circuito Exterior s/n CU, México D.F., 04510, Mexico
[b] Posgrado en Ciencia e Ingeniería de Materiales, UNAM, Unidad de Posgrado, Edificio C, Piso 1, Zona Cultural de CU, México, D.F., 04510, Mexico
[c] Laboratoire de Physique de la Matière Condensée, Université de Picardie Jules Verne, 33 rue Saint Leu, 80039, Amiens Cedex 1, France

ARTICLE INFO

Article history:
Received 1 September 2016
Received in revised form
14 November 2016
Accepted 23 November 2016
Available online 24 November 2016

Keywords:
Oxide materials
Thin films
Vapor deposition
Optical properties
X-ray diffraction
Photocatalytic evaluation

ABSTRACT

Bismuth-based oxides have gained attention because of their particular electronic configuration that enhances the mobility of photogenerated carriers. In this work, we focused on the synthesis, and the evaluation of the physical and photocatalytic properties of $Bi_5Nb_3O_{15}$ films. Bismuth niobate films were deposited by dual magnetron co-sputtering, starting from Bi_2O_3 and Nb independently driven targets. Although the substrates were heated at 150 °C during the deposition, the films were amorphous; therefore, they were annealed at 600 °C in air for 2 h to obtain the nanocrystalline $Bi_5Nb_3O_{15}$ orthorhombic phase. The $Bi_5Nb_3O_{15}$ compound is an interesting material for applications in microelectronics due to its high-k dielectric value at the radiofrequency range; another possible and reported application is as photocatalyst for degradation of organic pollutants and water splitting processes. The films structure was confirmed by X-ray diffraction (θ-2θ and in-plane modes). The Raman and infrared spectra were measured and compared with calculated vibrational modes since they have not been reported in the past. The optical properties (refractive index, extinction and absorption coefficients) of the $Bi_5Nb_3O_{15}$ films were estimated using UV–VIS reflectance and transmittance spectroscopy. The optical band gap was estimated assuming an indirect fundamental inter-band transition at 3.25 eV. The prospective to use the $Bi_5Nb_3O_{15}$ films as a photocatalyst was evaluated through the measurement of the photodiscoloration of indigo carmine (IC) dye solutions (5 ppm) under UV light irradiation at three pHs: 3.5, 7 and 11. The results showed a decrease in the absorbance spectrum of the IC solution as a function of irradiation time only at acidic pH where almost 100% of degradation was achieved at 270 min; this behavior is probably due to the increment of the adsorption of IC molecules on the positively charged surface. A similar response was observed after 5 cycles without any structural change of the films.

1. Introduction

Bismuth compounds are attractive because of their low toxicity, low cost and the facility to produced nanostructures with different shapes, morphology and size. Among the different bismuth complex oxides, the bismuth niobate phases have been less investigated. The $Bi_5Nb_3O_{15}$ compound is a high-k dielectric material that if obtained as a thin film has potential application as the dielectric material in metal-insulator-metal capacitors [1–3]. However, the synthesis of highly crystalline thin films has been proved difficult even when the starting target material has the right composition. Cho et al. [2] prepared different $Bi_xNb_yO_z$ (named as BNO) films by magnetron sputtering from a single $Bi_5Nb_3O_{15}$ target, obtaining the $Bi_5Nb_3O_{15}$ phase for deposition temperatures between 450 and 550 °C, while at higher temperatures the films had another bismuth niobate phase. Seong et al. [4] obtained crystalline BNO films by pulsed laser deposition (PLD) from a $Bi_5Nb_3O_{15}$ target working at a deposition temperature of 550 °C.

The $Bi_5Nb_3O_{15}$ structure was firstly described by Roth and Waring [5] as tetragonal; although they could not indexed all of the peaks in the XRD pattern taking the tetragonal structure and they recognized a possible pseudo-tetragonal distorted pyrochlore-like structure. Takenaka et al. [6] considered that the structure of this

* Corresponding author. Instituto de Investigaciones en Materiales, UNAM, Circuito Exterior s/n CU, México D.F., 04510, Mexico.
E-mail address: 21.juancarlos@gmail.com (J.C. Medina).

http://dx.doi.org/10.1016/j.jallcom.2016.11.340
0925-8388/

niobate was orthorhombic and related to the Aurivillius-phases, specifically as a mixed-layer Aurivillius-phase composed by two parts: $[(Bi_2O_2)^{2+}(NbO_4)^{3-}]$ and $[(Bi_2O_2)^{2+}(BiNb_2O_7)^{-}]$, and so they could indexed the XRD pattern according to an orthorhombic lattice. Tahara et al. [7] refined the $Bi_5Nb_3O_{15}$ structure from powder neutron diffraction patterns demonstrating the proposal of the above mentioned orthorhombic layered structure; they assigned it to the *Pnc*2 (No. 30) space group with $a = 2.1011(4)$, $b = 0.5473(1)$ and $c = 0.5463(1)$ nm. However, between these two authors [6,7], there is still some controversy about the proper indexation of the crystallographic planes and up to date, the vibrational Raman and IR spectra have not been reported.

We used the dual co-sputtering technique for the synthesis of the $Bi_5Nb_3O_{15}$ phase, starting from two independently driven targets, Bi_2O_3 and Nb. The sputtering deposition technique is a scalable low cost method; the films deposited by this technique are compact, have high quality, good adhesion to the substrate and uniformity. Multi-target sputtering allows an easy control of the film composition by varying the power applied to the targets [8–11].

On the other hand, the photocatalytic activity of the $Bi_5Nb_3O_{15}$ orthorhombic phase has been reported previously for powder samples. One of the pioneering works was done by Gurunathan et al. [12], who prepared particles of $Bi_5Nb_3O_{15}$ via a solid state reaction and evaluated the photocatalytic (PC) activity for water splitting under near visible-light, concluding that it has potential to be used for solar energy conversion. The photocatalytic properties of $Bi_5Nb_3O_{15}$ powders have been studied in comparison to $Ag/Bi_5Nb_3O_{15}$ [13] or $Pt/Bi_5Nb_3O_{15}$ [14] heterostructured systems. The effect of the metal co-catalyst was dual, to retard the electron-hole pair recombination by trapping the photo-induced conduction band electrons in the metal and to enhance the optical absorption of visible-light via the surface plasmon resonance. In those works [13,14], the photocatalytic activity was demonstrated for a flame retardant (tetrabromobisphenol A), methyl orange dye and *p*-nitrophenol solutions under different illumination wavelengths. Zhao et al. [15] evaluated the photocatalytic photodegradation of ornidazole solution using nanoparticles of Y^{3+}-doped $Bi_5Nb_3O_{15}$ under visible-light, the degradation efficiency of pure $Bi_5Nb_3O_{15}$ was 80.3% after 180 min, while the doped sample reached about 90.5%. Zhang et al. [16] evaluated the photocatalytic performance of heterojunctions of graphitic carbon nitride and the niobate for the degradation of methyl orange and 4-chlorophenol under visible-light irradiation; the conversion of methyl orange and 4-chlorophenol were 28% after 180 min and 38% after 60 min, respectively. Once again, the PC activity was improved by the formation of the heterojunction using carbon nitride, i.e. a common result is that the pure $Bi_5Nb_3O_{15}$ presents moderate photocatalytic activity but that it is sensitive to be improved by the addition of metallic nanoparticles or heterojunctions. All these results are related to powder samples and there is no information about the PC activity of $Bi_5Nb_3O_{15}$ thin films. The use of thin films would avoid the secondary process of filtration or separation that has to be implemented when powder samples are used.

The aims of this work are to demonstrate that it is possible to obtain crystalline $Bi_5Nb_3O_{15}$ thin films by co-sputtering from Bi_2O_3 and Nb targets driven independently, as well as evaluate their optical and photocatalytic properties. Moreover, to properly and completely characterize the film structure, theoretical calculations based on the structure proposed by Tahara et al. [7] were done to obtain the vibrational Raman and IR active modes. Finally, the photocatalytic response of the $Bi_5Nb_3O_{15}$ films for discoloration of indigo carmine (IC) dye was assessed under different pHs and UV-light irradiation.

2. Experimental procedures

2.1. Deposition of the films

The films were prepared by reactive magnetron co-sputtering from two targets: Bi_2O_3 (purity 99.9%) and metallic Nb (purity 99.95%), both of diameter 2 in; each magnetron had an independent power source, radiofrequency (RF) for the oxide target and DC for the metallic target. The magnetrons are placed 11 cm from the substrate and at 58° angle, so that both plasmas converge in the center area of the substrate holder. In order to obtain films with a homogeneous composition, the substrates are placed radially along a donut area of inner radius 2 cm and outer radius 5.5 cm, while the substrate holder is rotated (10 rpm). Within this donut, the thickness variation is between 5 and 10% but similar composition and structure can be obtained. The RF power applied to the Bi_2O_3 target was fixed at 30 W, while the DC power applied to the Nb target was 70 W. The deposition process was done under an $Ar:O_2$ atmosphere with gas flow ratio (standard centimeters cubic per minute, sccm) 16:4, and the working pressure was 0.7 Pa. The substrates were Corning® 7059 glass pieces of 2.5×1.25 cm^2, which were heated at 150 °C for 30 min before starting the deposition. Under these conditions, the single oxides lead to deposition rates of 6 nm min^{-1} and 4 nm min^{-1} for the delta-Bi_2O_3 phase [17] and the amorphous Nb_2O_5, respectively. These deposition conditions were selected after performing a complete characterization of the system varying the Ar/O_2 ratio, the power applied to both targets and the deposition temperature. It should be mentioned that other compositions and phases of the BNO system could be obtained and will be reported in a separate paper.

2.2. Film characterization

The thickness and root mean square roughness (RMS) of the films were measured using a Veeco stylus profilometer model Dektak 150. The surface and cross-section morphology was observed using a Jeol 7600F Field emission-scanning electron microscope (FE-SEM) with 5 kV, and the sample was covered with gold to avoid charge accumulation.

The crystalline structure was verified by X-ray diffraction (XRD) using a Rigaku diffractometer, model Ultima IV, equipped with Cu Kα radiation, in both parallel-beam θ-2θ and in-plane modes, acquisition step 0.02° and scanning speed 1° min^{-1}. In addition, the structure was verified by microRaman spectroscopy using an EnSpectra R532 spectrometer with laser wavelength 532 nm. Also, the films were evaluated by Fourier transform infrared (FT-IR) spectroscopy using a Thermo Scientific Nicolet 6700 FT-IR spectrometer equipped with an attenuated total reflectance (ATR) attachment; the spectrum was recorded between 400 and 4000 cm^{-1} with resolution 1 cm^{-1}.

The optical properties (band gap and complex refractive index) of the films were evaluated by UV–VIS transmittance and reflectance spectrometry using a UV–Visible Jasco V670. The geometric configuration of this equipment allowed the spectra acquisition from the same area of the sample for both the transmittance and reflectance measurements. The software CODE® was used to estimate the optical properties through the fitting of theoretical models to the experimental data. A bottom homogenous layer followed by a gradient (different proportion of voids) porous layer were assumed; the porous-film layers were modeled using the Bruggeman [18] effective medium. The film optical properties were parameterized using the Tauc-Lorentz model [19]. The optical band gap, E_g, was estimated under the assumption of parabolic conduction and valence bands around the absorption edge [20]. The E_g was estimated as the photon energy at which a linear fitting of the

$(\alpha E)^{1/2}$ function around the absorption edge equals zero.

The $Bi_5Nb_3O_{15}$ Raman and IR active modes were calculated assuming the structure extracted by Tahara et al. [7] from the Rietveld refinement of neutron diffraction patterns. Those results suggest that the orthorhombic crystalline structure can be seen as a mixed-layered Aurivillius-related phase $[Bi_2O_2] + [NbO_4] + [BiNb_2O_7]$, with weak interaction between the layers. Therefore, as a first approximation the vibrational spectra were calculated assuming each structure separately and considering that in the solid state, the position of the signal will not change drastically, but the intensity will increase. The vibrational spectra of the whole orthorhombic structure correspond to the sum of the IR and Raman spectra of the individual layers. Calculations related to the optimization of the geometry were undertaken using the Gaussian 09 implementation [21]. The geometry of the model was fully optimized with *Becke three parameter hybrid Lee-Yang-Parr functional,* B3LYP [22–24] using LANL2DZ (Los Alamos ECP plus DZ on Na-La) for metal atoms and D5DV (Dunning/Huzinaga valence double-zeta) basis sets for light atoms [25–27]. In order to verify the optimized minima, harmonic analyses were performed and local minima were identified (zero imaginary frequencies). The Raman and IR spectra were obtained at the same level of theory.

2.3. Photocatalytic evaluation

The photocatalytic activity of the $Bi_5Nb_3O_{15}$ films was evaluated by the evolution of the absorbance spectrum of an aqueous solution 5 ppm of indigo carmine dye ($C_{16}H_8N_2Na_2O_8S_2$) as a function of the irradiation time. The pH of the solution was varied in three regimes: acidic (pH = 3.5), neutral (pH = 7) and basic (pH = 11).

For the discoloration tests, each film (2.5 × 1.25 cm) was immersed in 10 mL of the dye solution that was initially stirred in the darkness for 30 min to obtain a good dispersion and reach adsorption-desorption equilibrium between the organic molecules and the surface of the films. Then, the films were exposed to the light while keeping the stirring. A UV light source with main emission centered in 365 nm and intensity 26 W/m^2 was used to evaluate the response of the material. The absorption spectra of the solution were measured every 30 min during 3 h using a Shimadzu UV-1800 UV–VIS spectrophotometer. The degradation efficiency of the films was calculated as follows (Eq. (1)):

$$\%\ Discoloration = \left(1 - \frac{A}{A_o}\right) \quad (1)$$

where A_o y A are the absorbance maxima of the dye before and after the irradiation time, respectively. When a good percentage of discoloration was obtained (>60%), total organic carbon (TOC) was measured at the beginning and the end of the experiment using a TOC-L SHIMADZU Total Organic Carbon analyzer and using the Non-Purgeable Organic Carbon (NPOC) method in the high sensibility mode. Moreover, the same sample was used in five occasions under the same experimental conditions to evaluate both the reproducibility and stability of the photocatalyst. At the end of the cycles, the film was evaluated again using XRD and Raman spectroscopy.

Similar, photocatalytic experiments were done using commercial Degussa P25 TiO_2 powder and δ-Bi_2O_3 films for comparative purposes.

2.4. Point of zero charge

In order to understand the effect of the pH on the photocatalytic activity, the point of zero charge (pzc) was measured. Briefly, the pzc of the $Bi_5Nb_3O_{15}$ thin films was obtained by a potentiometric titration experiment where 0.01 M of KCl was used as a background electrolyte [28]. The tritation was carried out from pH 3 to 12, adjusting the initial pH with 0.01 M HCl solution. Then 2 mL of 0.01 M NaOH solution were added and the change in the pH was measured using a potentiometer (Jeanway model 3540). Finally, from the plot of the change of pH as a function of aggregated NaOH volume, the pzc can be read as the inflection point [29,30].

2.5. Hydroxyl radical determination

Because the mineralization process occurs via the interaction of hydroxyl radicals (•OH) with the organic molecules, an alternative test for the photocatalytic activity is the determination of the formation of •OH radicals as consequence of the illumination of the semiconductor with the appropriate light source. The evaluation of the •OH radicals generated by the $Bi_5Nb_3O_{15}$ thin films in solution was done through the photoluminescence (PL) technique using coumarin as a probe molecule. Coumarin reacts with •OH to produce a highly fluorescent product; 7-hydroxycoumarin. This method relies on the photoluminescence signal at 456 nm of 7-hydroxycoumarin generated at the catalyst/water interface [31]. The $Bi_5Nb_3O_{15}$ film was immersed in 10 mL of an aqueous solution of coumarin (5×10^{-4} M), the initial pH value was adjusted with solution 2×10^{-3} M of HNO_3 to obtain a pH value of 3; the suspension was stirred for 30 min under dark conditions. Then it was irradiated by the UV lamp (365 nm), during 1 h, and aliquots were taken at 30 and 60 min. The fluorescence spectra of the coumarin solution were measured on a Fluorolog®-3 Horiba spectrofluorometer using an excitation lamp at 350 nm. The same test was done using commercial Degussa P25 TiO_2 powder as the standard photocatalytic material.

3. Results

3.1. $Bi_5Nb_3O_{15}$ structural characterization

The as-deposited films were amorphous as can be observed in Fig. 1(a), which is a characteristic of many oxide thin films. Therefore, the samples were annealed in the high temperature attachment of the X-ray diffractometer to obtain the in-situ XRD patterns as a function of the temperature, where it was found that at 600 °C, the orthorhombic $Bi_5Nb_3O_{15}$ phase could be obtained (Supplementary Information Fig. S1). Then, all the as-deposited samples were annealed into a tubular furnace at 600 °C for 2 h and in static air and the XRD patterns confirmed the formation of the $Bi_5Nb_3O_{15}$ phase. No diffusion of the glass elements (Si, Ba, B, Al) was observed into the annealed films by X-ray photoelectron spectroscopy depth profile (data not shown).

Fig. 1(b–c) shows the XRD patterns of the annealed films measured in two modes for a better characterization of the film structure; θ-2θ and in-plane. The positions of the reflections with the respective indexes according to the data provided by Tahara et al. [7] are also included. The structural information of the Tahara et al.'s [7] work is detailed in the inorganic crystalline structure database card ICSD #245707. The θ-2θ mode contains the diffraction peaks corresponding to the atomic planes parallel to the substrate, while the in-plane mode contains the peaks from the planes perpendicular to the substrate. It can be seen that the position of the experimental peaks in both measurement modes, matched with the calculated positions from Tahara et al. [7] and also with the JCPDS file 00-051-1752 file from Takenaka et al.'s work [6], the corresponding interplanar distances are also shown in Table 1. The good agreement between the database patterns and both experimental patterns allows us to make an accurate identification of the $Bi_5Nb_3O_{15}$ structure of the films. The diffraction peak intensities

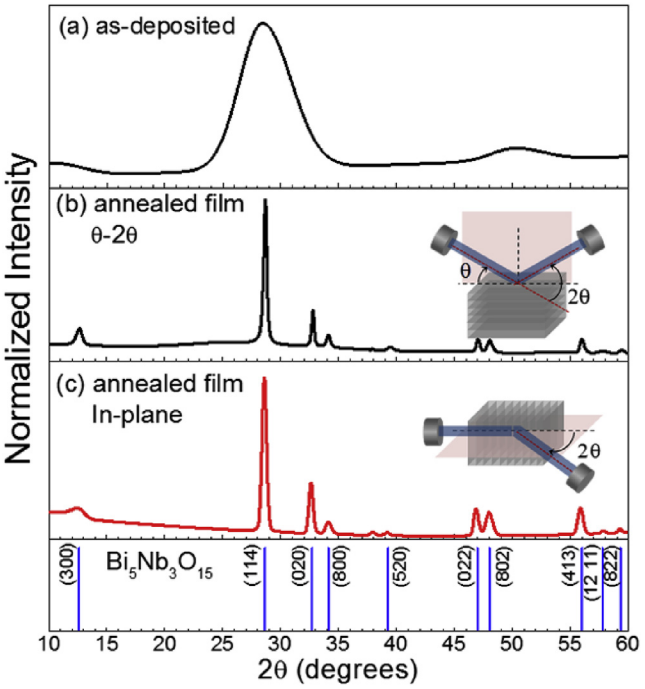

Fig. 1. XRD patterns of (a) as-deposited film, and the annealed film which were recorded using two measurements modes: (b) θ-2θ and (c) in-plane, and the reflection positions calculated from the Tahara et al.'s [7] work with the respective indexation.

were not estimated by Tahara et al. [7], however the fact that the relative intensity of the diffraction peaks in both modes (in-plane and θ-2θ) agreed very well is an indication that there is no a preferential orientation growth. This is different from previous reports of $Bi_5Nb_3O_{15}$ films, where not all the diffraction peaks are observed [2,4]. The crystalline domain was obtained using the Halder-Wagner method [32], which gives better precision than the Scherrer method because it takes into account all the diffraction peaks. The crystalline domain size for the annealed-films was 35 ± 4 nm.

The thickness and RMS roughness of the annealed-films were 288 ± 10 nm and 32 ± 9 nm, respectively.

Fig. 2 shows the surface morphology of the annealed films deposited on glass substrate. The image shows some flat grains with pores or cracks at certain regions. However, these grains are more probably related to the columnar film structure than to the crystalline domain size since the dimensions are very different; 100–250 nm for the SEM image versus 34 nm for the crystalline domain. The pores are probably formed during the annealing crystallization process, which involves atomic rearrangements during the nucleation and growth of the crystals with possible shrinkage of the structures. Furthermore, the different thermal expansion coefficients between the film and the substrate might also play a role. Nevertheless, when the cross-section of the tilted sample is observed (Fig. 2(b)), the film looks compact and uniform in thickness.

Table 1
Interplanar spacing from the XRD data of this work, Tahara et al.'s [7] and Takenaka et al.'s [6] works.

d (Å) – this work		d (Å)/(*hkl*) [7]	d (Å)/(*hkl*) [6]
θ-2θ	In plane		
6.987	7.070	7.004/(300)	
3.111	3.122	3.114/(411)	3.088/(114)
2.731	2.744	2.737/(020)	2.730/(200)
2.627	2.629	2.626/(800)	2.642/(202)
2.375	2.370		
2.284	2.296	2.293/(520)	
1.932	1.939	1.933/(022)	1.954/(01–10)
1.894	1.896	1.893/(802)	1.901/(221)
1.643	1.646	1.641/(413)	1.651/(02–10)
1.591	1.594	1.595/(1211)	
1.553	1.559	1.557/(822)	

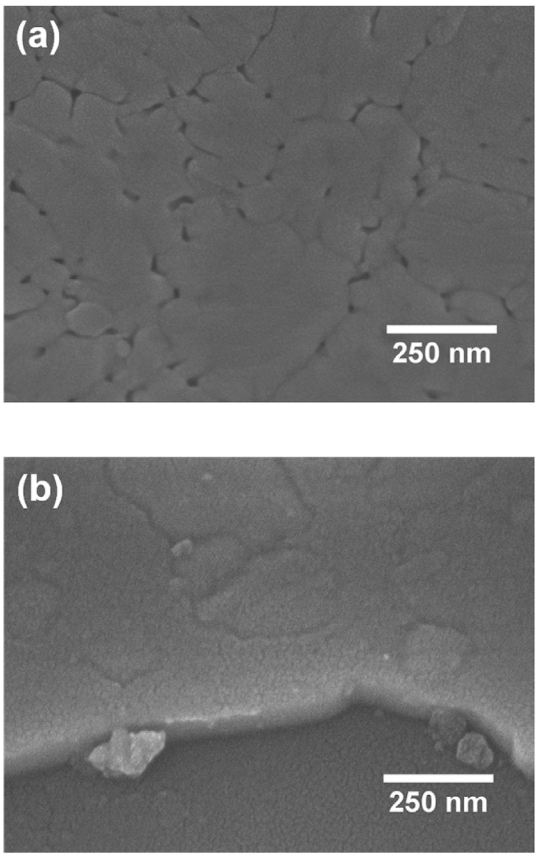

Fig. 2. SEM micrographs of the (a) top-surface and (b) cross-section of an annealed crystalline $Bi_5Nb_3O_{15}$ film deposited on glass. The film was covered with gold.

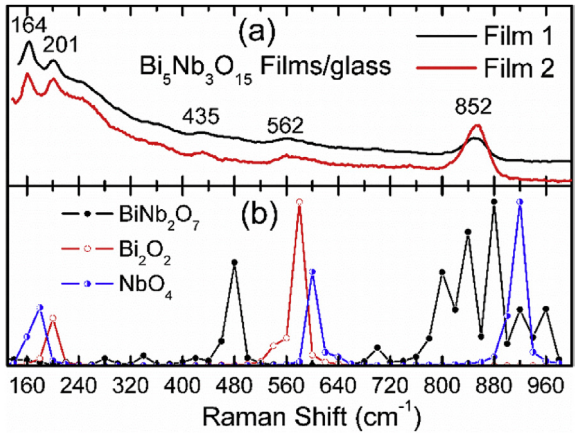

Fig. 3. (a) Experimental Raman spectra of two different $Bi_5Nb_3O_{15}$ films on Corning® 7059 glass, and (b) calculated Raman spectra corresponding to the three molecular groups which are comprised into the $Bi_5Nb_3O_{15}$ mixed-layered Aurivillius-related structure.

Table 2
Main calculated and experimental Raman and Infrared frequencies (in cm^{-1}) with their corresponding molecular groups Bi_2O_2, NbO_4, $BiNb_2O_7$. The discrepancy between theoretical an experimental Raman frequencies are also indicated.

Mode	Molecular group	Calculated		Experimental Raman [R] and infrared [IR]	Discrepancy
		Raman	Infrared		Raman modes
1	NbO_4	176	176	164[R]	13
2	Bi_2O_2	195		201 [R]	6
3	$BiNb_2O_7$	474		435 [R][a]	39
4	Bi_2O_2		492	480 [IR]	
5	Bi_2O_2	575		562 [R]	13
6	$BiNb_2O_7$		694	680 [IR]	
7	$BiNb_2O_7$	803	803	805 [IR]	
8	$BiNb_2O_7$	844	844	852 [R]; 860 [IR]	8
9	$BiNb_2O_7$	883		852 [R][a]	31
10	NbO_4	903	903	860 [IR]	

[a] The agreement is not very good.

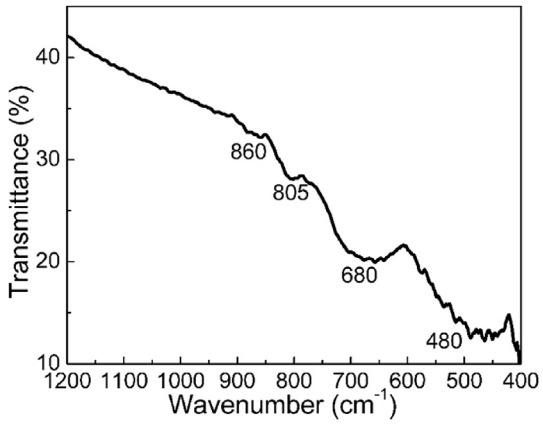

Fig. 4. FT-IR spectrum measured in ATR mode.

As a complementary tool to correctly identify the structure of the films, the Raman and infrared spectra were calculated using the atomic position from the proposal of Tahara et al. [7]. The micro-Raman spectra was used as a tool to corroborate the uniformity of the films but also as a quick test to observed the reproducibility of the deposition-annealing process to obtain the $Bi_5Nb_3O_{15}$ phase. Fig. 3 (a) shows that the spectra obtained from films obtained in different deposition runs are very similar. Comparison between the calculated and measured Raman spectra is also shown in Fig. 3 (b), while the corresponding frequencies are reported in Table 2. The experimental Raman spectra presented a strong photo-luminescence background which hides some low intensity peaks. The frequency of the most intense experimental Raman bands were estimated using a Lorentz fitting after background subtraction and are positioned around 164 (assigned to mode 1), 201 (mode 2), 435 (possibly mode 3), 562 (mode 5) and 852 (modes 8 and possibly mode 9) cm^{-1}. As can be seen, there is a fairly good agreement between calculated and experimental spectra (maximum discrepancy 39 cm^{-1}) despite that the theoretical optimization is done in the gas phase, while the structure correspond to a solid structure. The assignment of the experimental bands to the calculated atom displacements was performed through a comparison between both spectra not paying attention to the intensity of the peaks, but only to their relative wavenumbers. It is well known that the intensity of the Raman spectra depends on too many external factors such as the uniformity of the sample and the geometric arrangement between the laser and the angle of diffraction, while the intensity of the signal cannot be properly simulated by this level of calculations.

For the IR spectrum (Fig. 4), broad-low intensity signals were observed, making more difficult the estimation of the discrepancy value. However, it is possible to identify some relationships; the broad-weak bands centered around 860 cm^{-1} are assigned to the overlapping of the mode 8 from the $BiNb_2O_7$ cluster and mode 10 of the NbO_4 polyhedra. The band centered around 805 cm^{-1} is assigned to the mode 7 and the very broad and intense 680 cm^{-1} band to the mode 6, both of the $BiNb_2O_7$ group. Finally, the 480 cm^{-1} band is assigned to mode 4 of the Bi_2O_2. The broad IR

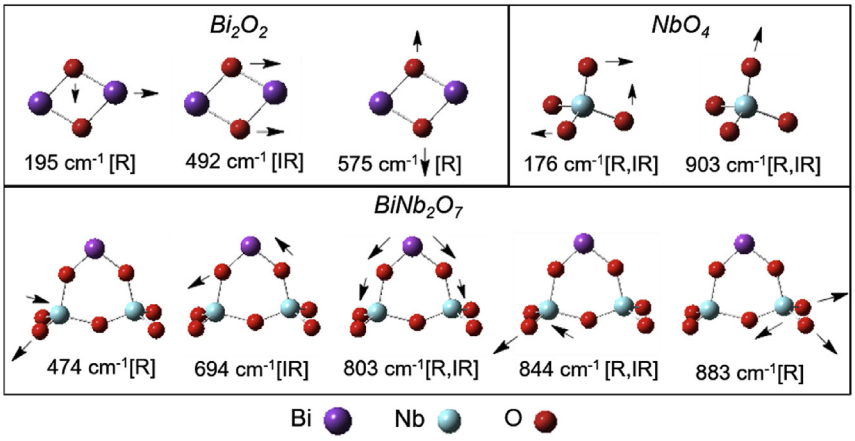

Fig. 5. Atomic displacements of the three constituent groups of the $Bi_5Nb_3O_{15}$ mixed-layer Aurivillius-related structure, which originate the mean active vibrational modes in Raman [R] and infrared [IR] spectra of the bismuth niobate.

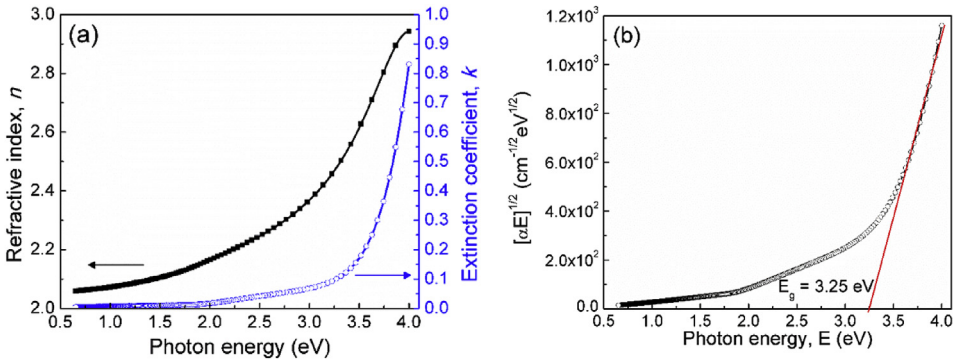

Fig. 6. Optical properties of a $Bi_5Nb_3O_{15}$ films calculated from the UV–VIS spectrometry: (a) the refractive index and extinction coefficient spectra, and (b) the graphical estimation of the band gap considering the fundamental transition as indirect.

bands at 600 and 800 cm^{-1} were also observed by Zhang et al. [16] for the $Bi_5Nb_3O_{15}$ powders, but no explanation was given.

The atomic vibrational displacements corresponding to the modes described in Table 2 are shown in Fig. 5.

3.2. Optical properties

The most common optical property reported of the $Bi_5Nb_3O_{15}$ phase is the optical band gap, which is easily obtained from a diffuse reflectance analysis of the powder samples, but that do not allow the estimation of the absolute absorption coefficient or the complex refractive index. The optical functions of the films (refractive index n, and extinction coefficient k) were estimated from the fitting of the Reflectance and Transmittance spectra (Fig. S2), and the optical band gap from the estimation of the absorption coefficient α (cm^{-1}) using Eq. (2)

$$\alpha\left(cm^{-1}\right) = \frac{4\pi k}{\lambda(cm)} \tag{2}$$

where λ is the wavelength. The spectra of the real and the imaginary parts of the complex dielectric function are shown in Fig. S3.

Fig. 6 shows the optical functions of the $Bi_5Nb_3O_{15}$ films: (a) the refractive index and extinction coefficient as a function of the photon energy and (b) the plot used to estimate the optical band gap. Fig. 6 (a) shows the high refractive index of the films which make them interesting for optical and electronic applications. The extinction coefficient is very low for energies below 3.0 eV and then increases rapidly after the absorption edge. The estimation of the band gap (Fig. 6(b)) was done using the model for indirect band transitions around the absorption edge, leading to a value of 3.25 ± 0.10 eV, where the error was estimated making the same calculation for more than one sample and by varying slightly the energy limits used to perform the linear fitting. This data indicates that the material will be active for photocatalysis only under UV illumination.

3.3. Point of zero charge, pzc

The measured pzc for the $Bi_5Nb_3O_{15}$ films is 7.8, which has not been reported previously (Supplementary Information Fig. S4). For the δ-Bi_2O_3 films, the pzc obtained in our group was 8 [33] and for the P25 TiO_2 Degussa particles, it has been reported as 6 [34]. The pH of point of zero charge is an important property of the surfaces because depending on the pH of the solution, it defines the ability of the surface to adsorb anionic or cationic molecules when they are dispersed into aqueous solution. When the pH is below the pzc value, the solid surface becomes protonated [35], and anionic molecules can be adsorbed.

3.4. Photocatalytic discoloration experiments

Fig. 7 shows the absorbance of the indigo carmine dye solution (starting concentration 5 ppm) as a function of the UV irradiation time for the three pH values. The characteristic absorbance peak of the IC dye at 610 nm [36] insignificantly decrease during the dark condition (30 min) for the three pHs, suggesting that a very small amount of the IC dye was permanently adsorbed on the film surface. Fig. 7 also shows that degradation occurs only at acidic pH (Fig. 7 (a)) reaching nearly 100% at 270 min, while at neutral and basic pHs, the degradation is minimal. As suggested by the pzc value (pzc = 7.8) of the $Bi_5Nb_3O_{15}$, at the IC dye solution (neutral) and the basic pH, the surface charge of the $Bi_5Nb_3O_{15}$ samples must be poorly protonated and as result, the IC dye could not be adsorbed in the region of the surface amphoteric sites. Thus, the interaction of the anionic dye with the poorly protonated surface is only due to hydrogen bonds and, as consequence, the dye adsorption and degradation is weak [37], contrary to the situation at acidic pH. For this acidic condition, the films surface will be highly protonated enhancing the adsorption of the IC molecule and leading to destruction of its indigoid group (NHC=CNH) via oxidation. The formation of secondary products is also observed through the increase in the absorbance below 240 nm. Indeed, for the acidic conditions, a clear isosbestic point (inset in Fig. 7(a)) can be observed at 252 nm, indicating the increase of the secondary products at lower wavelengths which have been identified as *Isatin sulfonic acid and 2-amine-5-sulfo-benzoic acid* [36,38–40]. However, the bands associated to the secondary products cannot be clearly observed in the spectra due to interferences with the nitric acid used to reduce the pH, meanwhile they are clearly observed for the neutral pH. The presence of the isosbestic point showing the increment in the secondary products without their further

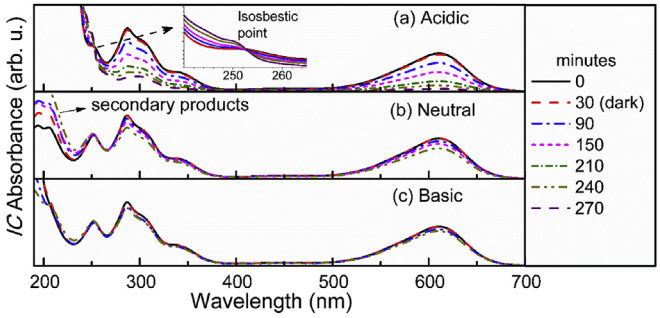

Fig. 7. Absorbance spectra of the IC dye solution as a function of the UV irradiation time in different pHs: (a) acidic 3.5, (b) neutral 7 and (c) basic 11. The inset in (a) shows the detail of the isosbestic point.

reduction, is an indication that the mineralization of the IC dye was not complete during the evaluation time [39].

Fig. 8 shows the profile of relative concentration (C/C_o) as a function of the irradiation time for the photolysis (no semiconductor added), the $Bi_5Nb_3O_{15}$ film, a δ-Bi_2O_3 film and Degussa P25 TiO_2 powder, all of them measured at acidic pH (where according to their pzc values, the adsorption of the IC molecule is favored). The Bi_2O_3 were deposited by a similar method and is used only for comparative reasons to show that the unusual C/C_o decay is not characteristic of thin films [33,41]. Fig. 8 shows that the $Bi_5Nb_3O_{15}$ film induced a linear degradation of the IC dye molecule, different to the behavior observed for the Bi_2O_3 film and the P25 TiO_2 powder. This linear plot is an indication that the Langmuir-Hinshelwood approximation should not be used to estimate the reaction rate, such linear response has also been observed in previous works using powder nanostructures [14,16]. Furthermore, Fig. 8 shows that in comparison to the Bi_2O_3 thin films studied in our group [33,41], the discoloration activity is significantly lower on the $Bi_5Nb_3O_{15}$ samples. Both films showed lower C/C_o reduction than the P25-TiO_2 partially as a consequence of the reduced surface area of the films in comparison to a nanometric powder. However, as shown below, also it was due to the lower efficiency of the films to produce the hydroxyl radicals.

The photodiscoloration experiments using the same $Bi_5Nb_3O_{15}$ film were repeated five cycles observing that the decrease in the relative concentration was always the same, reaching 100% discoloration in 270 min (Shown in Fig. S5), suggesting a good stability of the films. The stability was confirmed by XRD and Raman spectroscopy showing that the films did not change during the five photocatalytic tests (Supplementary Information Fig. S6.)

Despite that the photodegradation experiments showed a decrease of nearly 100% (270 min) of absorbance using the acidic pH, the total organic carbon was not reduced, in agreement with the formation and increase of the intermediary products observed in Fig. 7. This was also confirmed by the evaluation of the creation of •OH radicals. Fig. 9 shows the PL spectra of the coumarin solution aliquots after 30 and 60 min for the films and the TiO_2 standard nanoparticles (Degussa P25), where it is clearly observed that the films presented two orders of magnitude less •OH radical formation than the TiO_2.

4. Discussion

The synthesis of films from the BNO system has been investigated mainly in the search for high-k dielectrics that could

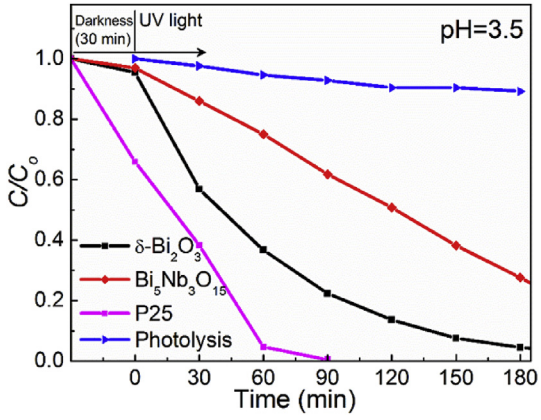

Fig. 8. Profile of relative concentration (C/C_o) of the IC solution aliquots at acidic pH (3.5) as a function of the UV irradiation time for the photolysis (no film immersed), the $Bi_5Nb_3O_{15}$ film, the δ-Bi_2O_3 film and Degussa P25 TiO_2 powder.

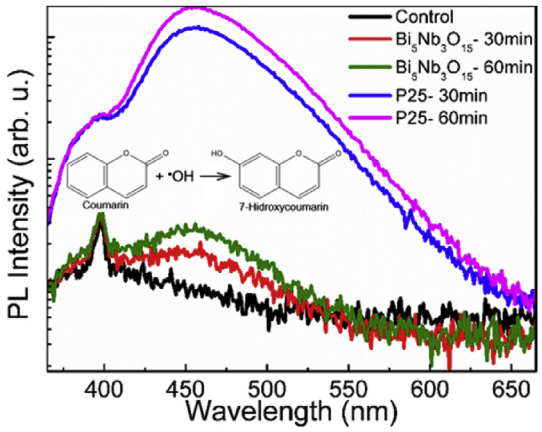

Fig. 9. Photoluminescence spectra of coumarin solution aliquots at acidic pH as a function of the irradiation time during the interaction with a $Bi_5Nb_3O_{15}$ film and Degussa P25 TiO_2 powder.

substitute SiO_2 or Si_3N_4 in the metal-insulator-metal capacitors [1]. In principle because it is argued that crystalline BNO films could be obtained at relative low synthesis temperatures [2]. Nevertheless, as described in the introduction, the synthesis of purely crystalline $Bi_5Nb_3O_{15}$ orthorhombic phase films (the compound with the higher dielectric constant) at low temperatures (below 400 °C) has not been very successful. This work is not the exception, we have demonstrated that the production of the orthorhombic $Bi_5Nb_3O_{15}$ phase as thin film is possible by co-sputtering from two independent targets, but again post-annealing treatment at 600 °C was required. This temperature is comparable to those reported by Seong et al. [4] using pulsed laser deposition (PLD) from a $Bi_5Nb_3O_{15}$ target, where the crystalline films were obtained using deposition temperatures between 500 and 550 °C. Similarly, for the films deposited by sputtering from a single $Bi_5Nb_3O_{15}$ target [2], crystalline $Bi_5Nb_3O_{15}$ films were only obtained at substrate temperatures of 450–550 °C.

Nonetheless, it is important to mention that in contrast to the previous works about the synthesis of $Bi_5Nb_3O_{15}$ films, the XRD patterns in our case showed a clear coincidence with Tahara et al.'s [7] report. The two identical patterns obtained from the two diffraction modes (θ-2θ and In-plane) clearly demonstrated that the films are composed of randomly oriented $Bi_5Nb_3O_{15}$ nanograins. Moreover, Raman and infrared spectroscopies were also used as techniques to identify the structure of the films comparing the results with theoretically calculated spectra. There was a fairly good agreement and 9 of 10 theoretical modes could be identified. One interesting result is that the Raman active band observed around 850 cm^{-1}, that was the most intense for all the samples independently of the substrate or Raman configuration, could be used as a signature of the $Bi_5Nb_3O_{15}$ orthorhombic phase. This band is probably the convolution of more than one vibrational mode but has not been observed in the spectra of the $BiNbO_4$ polymorphs [42,43], which are characterized by a Raman intense band around 610-630 cm^{-1}. No comparison to other BNO compounds can be done since the vibrational spectra have not been reported for either the Bi_3NbO_7 compound or the solid solutions.

Another contribution from this work is the estimation of the optical properties of the $Bi_5Nb_3O_{15}$ orthorhombic phase. Kang et al. [44] used ellipsometry to obtain the (n, k) functions of bismuth niobates films deposited by PLD, but they could not obtain the $Bi_5Nb_3O_{15}$ phase [44]. On the contrary, in our case, we have clearly demonstrated the formation of the $Bi_5Nb_3O_{15}$ phase, and comparison between both works suggests that the optical properties are

similar among the different compounds and phases of the BNO system. The $Bi_5Nb_3O_{15}$ films showed high refractive index ranging from 2.06 at 0.65 eV to 2.94 at 4.0 eV, with a similar trend to those reported by Kang et al. [44], such values are for sure of interest for photonics applications. The *k* values were used to calculate the absorption coefficient (Eq. (2)) and from there the optical band gap (E_g). Kang et al. [44] did not estimated the E_g for the other related BNO phases (amorphous, Bi_3NbO_7 and $BiNbO_4$), but by looking the *k* vs. energy spectra, it can be deduced that all films will have an optical band gap above 3.0 eV. This value is slightly larger to those reported for the $Bi_5Nb_3O_{15}$ powders [13–16]. In those papers, the estimation of the optical band gap is done using the Kubelka-Munk function obtained from the UV–VIS diffused reflectance spectra and the band gap are estimated assuming direct interband transition. The reported values are around 2.90 [16] –2.98 [15] eV.

In our experience working with nanocrystalline thin films, the indirect band gap model is regularly used to take into consideration the large component of grain boundaries that constitute defects states which absorb light at photon energies below the gap [17,45] and therefore, it is common that the band gap of the films is lower that the gap reported for powder samples. However, in this case, we have the opposite behavior without a clear explanation. Indeed the estimation of the direct band gap for the $Bi_5Nb_3O_{15}$ thin films lead to values around 3.7 eV, not realistic considering that the optical transmittance of the samples decreased at lower energies (Fig. S2). The tail of absorption at energies <3.0 eV is associated to structural defects, such as the grain boundaries or vacancies. Therefore, we conclude that the band gap estimation is fairly good and this suggests that the nominal band gap of a pure crystalline $Bi_5Nb_3O_{15}$ sample should be larger than the values reported for the powder samples and the values obtained for these nanocrystalline thin films. Granting that the definition of an absolute value of E_g is never easy to obtain since it depends on too many experimental parameters and the model used, as was observed years ago for the amorphous silicon thin films [46], we consider that there is also a problem with the proper identification of the $Bi_5Nb_3O_{15}$ phase reported for the powder samples. Analyzing carefully the diffraction patterns reported by Guo et al. [13,47] and Gurunathan et al. [12], it is clear that many diffraction peaks are not identified and do not belong to the $Bi_5Nb_3O_{15}$ phase, no matter the standard XRD pattern used. The presence of impurities in those powders could explain the lower band gap, as has been shown when metallic atoms are intentionally included in the structure [48,49]. This discrepancy in the estimation of the E_g might be seen as an insignificantly small numeric difference but it has large implications for the application. The relevance is that the E_g values are around the limit between visible (powders) and UV light (our films). Obviously, the threshold energy for the generation of photocarriers is a very important parameter for the possible application of the material as a visible-light photocatalyst and this can be strongly affected by impurities, either intentionally added or left as residuals during the synthesis process.

As described in the introduction, the previous reports about the visible-light driven photocatalysis using $Bi_5Nb_3O_{15}$ powders have included Ag, Pt, Y^{3+} or g-C_3N_4 in order to improve the activity in the visible range. In this paper, the photocatalytic evaluation of the $Bi_5Nb_3O_{15}$ films was done using a simplified method observing the degradation of a dye molecule through the measurement of the decrease in the absorbance of the dye solution. The catalyst to dye concentration ratio was in the similar order of magnitude (10^4 g/mol) that those reported by previous works [13,14,16]. However, in those works the sample were in powder form, so the surface area is much larger than our thin films.

In agreement, to our estimation of the optical band gap, the material did not show any photocatalytic activity using visible-light (data not shown). However, when the sample was illuminated using UV-light (365 nm – 3.4 eV), the IC dye degradation was possible, but highly dependent on the pH of the solution. Moreover, we confirmed that the IC dye was not degraded under UV illumination neither without the $Bi_5Nb_3O_{15}$ films nor in the dark in the presence of the films. The degradation was only observed under acidic pH (nearly 100% at 270 min) and according to the estimation of the pzc value, the response is explained in terms of an enhanced adsorption of the pollutant on the surface of the films, leading to a more efficient degradation of the molecule through interaction with the photogenerated carriers. Nevertheless, the TOC experiments, the evaluation of •OH radical formation by illumination of the $Bi_5Nb_3O_{15}$ films, as well as the increase in the absorbance of the secondary products (*Isatin sulfonic acid* and *2-amine-5-sulfo-benzoic acid)* with the irradiation time, are clear indications that the dye mineralization was not completed. A possible explanation for these results can be elaborated considering the relative position of the conduction and valence bands of the material. In order to measure the position of the conduction band, it is required that the film is deposited on a transparent conductive oxide, but as a first approximation, it is also possible to assess it conceptually. Based on the empirical approximation of Scaife [16,50], which is valid for oxide materials with completely full (d^{10}) or empty (d^0) *d* electronic states, the position of the conduction band minimum can be approximated by $V_{CB} = 2.94 - E_g$ (vs normal hydrogen electrode, NHE), where the 2.94 is an empirical value and E_g is the optical band gap. The V_{CB} of the $Bi_5Nb_3O_{15}$ films (which fulfill the previous requirements) using this equation and the optical band gap determined in this work, is at –0.31 V (vs NHE). Then, a band diagram scheme (Fig. 10) can be produced to understand the observed results related to the photodiscoloration of the IC dye without mineralization and the low •OH yielded.

According to the diagram, the band positions of the $Bi_5Nb_3O_{15}$ films are very similar to the TiO_2 and so both oxidation and reduction reactions induced by the photogenerated carriers e^-_{CB} and h^+_{VB} are energetically favorable at photon energies above the band gap, i. e. below 380 nm (UV light). However, we did not observed the creation of hydroxyl radicals as with the TiO_2, suggesting that the low photocatalytic activity observed must be related to a very high recombination rate of the $e^-_{CB} - h^+_{VB}$ pairs. The recombination process, although it needs further confirmation, could explain the dissimilar results in comparison to the $Bi_5Nb_3O_{15}$ powders, since one of the strategies to decrease the bulk

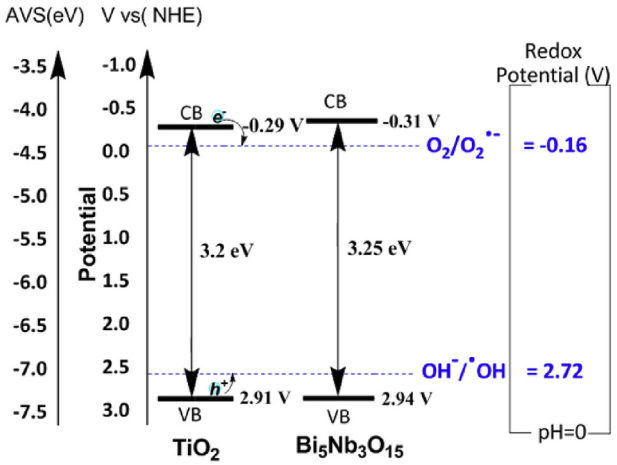

Fig. 10. Schematic energy level of the $Bi_5Nb_3O_{15}$ in comparison to the titanium oxide at pH = 0. The conduction band (CB) position of the $Bi_5Nb_3O_{15}$ was estimated using the approximation from Scaife [50].

recombination rate and increase the life-time of the photogenerated carriers is the reduction of the particle sizes, as those reported for the $Bi_5Nb_3O_{15}$ [13,15,16]. Similarly, the addition of noble metals diminishes the recombination rate because the metal particles act as electron acceptors and increase the separation of the photogenerated $e^-_{CB} - h^+_{VB}$ pairs, explaining the good photocatalytic activity of the Ag or Pt modified $Bi_5Nb_3O_{15}$ samples [13,14]. According to Sun and Wang [51], the extreme recombination is a common problem with bismuth based complex oxides despite their high photooxidation ability.

5. Conclusions

$Bi_5Nb_3O_{15}$ thin films were successfully prepared by a dual co-sputtering process that does not require the synthesis of special targets with the same composition. The combined characterization of XRD (θ-2θ and in-plane modes) and vibrational spectroscopies allow a complete identification of the structure that exhibits high crystallinity and phase purity. The simulation method at the density functional theory level with B3LYP functional using the LANL2DZ for metal atoms and D5DV basis sets for light atoms provides total Raman and IR spectra of the layered Aurivillius structure of the $Bi_5Nb_3O_{15}$ phase that matches quite well the experimental data. Reflectance and Transmittance spectroscopy was used to determine the optical properties of the $Bi_5Nb_3O_{15}$ films in the 0.65–4.0 eV spectral region using a Tauc-Lorentz model to parameterize the *n* and *k* functions. The high values of the refractive index (2.0–3.0) suggest that the material could be useful for photonic applications. Nevertheless, the high temperature of the annealing treatment used to obtain the phase might limit the possible applications. The threshold absorption energy or optical band gap was established at photon energies at 3.25 eV, i. e. in the UV spectral region. Therefore, in order to use the films as a visible-light photocatalyst, band engineering is required. The photodiscoloration (~100% in 270 min) of indigo carmine solutions (5 ppm) was achieved using low energy consumption (26 W/m^2) when the pH is reduced below the point of zero charge of the material, measured as $pH_{pzc} = 7.8$. However, no significant mineralization and production of •OH radicals was achieved indicating that despite the effective UV activated generation of the electron-hole carriers, there is a large bulk (within the film thickness) recombination limiting the degradation of organic pollutants.

Acknowledgments

This work was funded by the CONACYT-Project (No. 251279), PHOCSCLEEN 318977 and DGAPA-PAPIIT (IN100116). O.D-R and J.C.M. kindly acknowledge the National Council for Science and Technology (CONACYT) for the Ph.D. scholarship. The authors thank the support of the academic technicians Adriana Tejeda, Omar Novelo, Josué Romero, Hermilo Zarco, and Anna Cantaluppi-Harlé. This work was carried out using a NES supercomputer, provided by Dirección General de Cómputo y Tecnologías de Información y Comunicación (DGTIC), Universidad Nacional Autónoma de México (UNAM).

Appendix A. Supplementary data

Supplementary data related to this article can be found at http://dx.doi.org/10.1016/j.jallcom.2016.11.340.

References

[1] K.H. Cho, C.H. Choi, K.P. Hong, J.Y. Choi, Y.H. Jeong, S. Nahm, C.Y. Kang, S.J. Yoon, H.J. Lee, Electrical properties of amorphous $Bi_5Nb_3O_{15}$ thin film for RF MIM capacitors, IEEE Electr. Device Lett. 29 (2008) 684–687.
[2] K.-H. Cho, C.-H. Choi, Y.H. Jeong, S. Nahm, C.-Y. Kang, S.-J. Yoon, H.-J. Lee, Structural and electrical properties of $Bi_5Nb_3O_{15}$ thin films for MIM capacitors with low processing temperatures, J. Electrochem. Soc. 155 (2008) G148–G151.
[3] T.-G. Seong, K.-H. Cho, J.-W. Sun, M.-E. Song, D.-S. Paik, S. Nahm, C.-Y. Kang, J.-H. Kim, Crystallization and improvement of electrical properties of $Bi_5Nb_3O_{15}$ thin films grown at low temperature, Jpn. J. Appl. Phys. 48 (2009) 111401.
[4] T.G. Seong, K.H. Cho, J.Y. Choi, S. Nahm, C.Y. Kang, S.J. Yoon, J.H. Kim, Effects of oxygen pressure and Mn-doping on the electrical and dielectric properties of $Bi_5Nb_3O_{15}$ thin film grown by pulsed laser deposition, J. Phys. D. Appl. Phys. 42 (2009) 175402.
[5] R.S. Roth, J.L. Waring, Phase equilibrium relations in binary system bismuth sesquioxide-niobium pentoxide, J. Res. Natl. Bur. Stand., Sect. A 66 (1962) 451–463.
[6] T. Takenaka, K. Komura, K. Sakata, Possibility of new mixed bismuth layer-structured ferroelectrics, Jpn. J. Appl. Phys. 35 (1996) 5080–5083.
[7] S. Tahara, A. Shimada, N. Kumada, Y. Sugahara, Characterization of $Bi_5Nb_3O_{15}$ by refinement of neutron diffraction pattern, acid treatment and reaction of the acid-treated product with n-alkylamines, J. Solid State Chem. 180 (2007) 2517–2524.
[8] R. Mirabal-Rojas, O. Depablos-Rivera, S.M. Thalluri, J.C. Medina, M. Bizarro, J. Perez-Alvarez, S.E. Rodil, A. Zeinert, Effect of the KOH chemical treatment on the optical and photocatalytic properties of $BiVO_4$ thin films, Appl. Phys. A 122 (2016) 325.
[9] Y.R. Sui, Y.J. Wu, Y.P. Song, S.Q. Lv, B. Yao, X.W. Meng, L. Xiao, A study on structural formation and optical properties of $Zn_{1-x}Cd_xO$ thin films synthesized by the DC and RF reactive magnetron co-sputtering, J. Alloys Comp. 678 (2016) 383–388.
[10] X. Wang, X. Su, F. Hu, L. He, L. He, Z. Zhang, W. Zhao, K.-G. Wang, S. Wang, Growth $Al_xGa_{1-x}N$ films on Si substrates by magnetron sputtering and high ammoniated two-step method, J. Alloys Comp. 667 (2016) 346–351.
[11] K. Cheng, Y. Huang, J. Liu, M. Xue, Z. Kuang, Z. Lu, S. Wu, Z. Du, Chalcogenide solar cells fabricated by co-sputtering of quaternary $CuIn_{0.75}Ga_{0.25}Se_2$ and in targets: another promising sputtering route for mass production, J. Alloys Comp. 684 (2016) 237–244.
[12] K. Gurunathan, P. Maruthamuthu, $Bi_5Nb_3O_{15}$ as a photocatalyst: photocatalytic and photoelectrochemical studies, J. Solid State Electrochem. 2 (1998) 176–180.
[13] Y.N. Guo, L. Chen, X. Yang, F.Y. Ma, S.Q. Zhang, Y.X. Yang, Y.H. Guo, X. Yuan, Visible light-driven degradation of tetrabromobisphenol A over heterostructured $Ag/Bi_5Nb_3O_{15}$ materials, RSC Adv. 2 (2012) 4656–4663.
[14] L. Chen, W. Guo, Y.X. Yang, A. Zhang, S.Q. Zhang, Y.H. Guo, Y.N. Guo, Morphology-controlled preparation and enhanced simulated sunlight and visible-light photocatalytic activity of $Pt/Bi_5Nb_3O_{15}$ heterostructures, Phys. Chem. Chem. Phys. 15 (2013) 8342–8351.
[15] J. Zhao, B.H. Yao, Q. He, T. Zhang, Preparation and properties of visible light responsive Y^{3+} doped $Bi_5Nb_3O_{15}$ photocatalysts for Ornidazole decomposition, J. Hazard. Mater. 229 (2012) 151–158.
[16] S.Q. Zhang, Y.X. Yang, Y.N. Guo, W. Guo, M. Wang, Y.H. Guo, M.X. Huo, Preparation and enhanced visible-light photocatalytic activity of graphitic carbon nitride/bismuth niobate heterojunctions, J. Hazard. Mater. 261 (2013) 235–245.
[17] C.L. Gomez, O. Depablos-Rivera, P. Silva-Bermudez, S. Muhl, A. Zeinert, M. Lejeune, S. Charvet, P. Barroy, E. Camps, S.E. Rodil, Opto-electronic properties of bismuth oxide films presenting different crystallographic phases, Thin Solid Films 578 (2015) 103–112.
[18] D.A.G. Bruggeman, Calculation of various physics constants in heterogeneous substances I Dielectricity constants and conductivity of mixed bodies from isotropic substances, Ann. Phys. - Berl. 24 (1935) 636–664.
[19] G.E. Jellison, F.A. Modine, Parameterization of the optical functions of amorphous materials in the interband region, Appl. Phys. Lett. 69 (1996) 371–373.
[20] M. Bizarro, S.E. Rodil, Physicochemical characterization of photocatalytic materials, in: A. Hernández-Ramírez, I. Medina-Ramírez (Eds.), Photocatalytic Semiconductors: Synthesis, Characterization, and Environmental Applications, Springer International Publishing, Cham, 2015, pp. 103–153.
[21] M.J. Frisch, G.W. Trucks, H.B. Schlegel, G.E. Scuseria, M.A. Robb, J.R. Cheeseman, G. Scalmani, V. Barone, B. Mennucci, G.A. Petersson, H. Nakatsuji, M. Caricato, X. Li, H.P. Hratchian, A.F. Izmaylov, J. Bloino, G. Zheng, J.L. Sonnenberg, M. Hada, M. Ehara, K. Toyota, R. Fukuda, J. Hasegawa, M. Ishida, T. Nakajima, Y. Honda, O. Kitao, H. Nakai, T. Vreven, J.A. Montgomery Jr., J.E. Peralta, F. Ogliaro, M.J. Bearpark, J. Heyd, E.N. Brothers, K.N. Kudin, V.N. Staroverov, R. Kobayashi, J. Normand, K. Raghavachari, A.P. Rendell, J.C. Burant, S.S. Iyengar, J. Tomasi, M. Cossi, N. Rega, N.J. Millam, M. Klene, J.E. Knox, J.B. Cross, V. Bakken, C. Adamo, J. Jaramillo, R. Gomperts, R.E. Stratmann, O. Yazyev, A.J. Austin, R. Cammi, C. Pomelli, J.W. Ochterski, R.L. Martin, K. Morokuma, V.G. Zakrzewski, G.A. Voth, P. Salvador, J.J. Dannenberg, S. Dapprich, A.D. Daniels, Ö. Farkas, J.B. Foresman, J.V. Ortiz, J. Cioslowski, D.J. Fox, Gaussian 09, Gaussian, Inc., Wallingford, CT, USA, 2009.
[22] A.D. Becke, Density-functional thermochemistry. III. The role of exact exchange, J. Chem. Phys. 98 (1993) 5648–5652.
[23] C. Lee, W. Yang, R.G. Parr, Development of the Colle-Salvetti correlation-energy formula into a functional of the electron density, Phys. Rev. B 37 (1988) 785–789.
[24] B. Miehlich, A. Savin, H. Stoll, H. Preuss, Results obtained with the correlation

energy density functionals of becke and Lee, Yang and Parr, Chem. Phys. Lett. 157 (1989) 200–206.
[25] P.J. Hay, W.R. Wadt, Ab initio effective core potentials for molecular calculations. Potentials for the transition metal atoms Sc to Hg, J. Chem. Phys. 82 (1985) 270–283.
[26] P.J. Hay, W.R. Wadt, Ab initio effective core potentials for molecular calculations. Potentials for K to Au including the outermost core orbitals, J. Chem. Phys. 82 (1985) 299–310.
[27] W.R. Wadt, P.J. Hay, Ab initio effective core potentials for molecular calculations. Potentials for main group elements Na to Bi, J. Chem. Phys. 82 (1985) 284–298.
[28] A. Naveau, F. Monteil-Rivera, J. Dumonceau, S. Boudesocque, Sorption of europium on a goethite surface: influence of background electrolyte, J. Contam. Hydrol. 77 (2005) 1–16.
[29] J.J. Gulicovski, L.S. Čerović, S.K. Milonjić, Point of zero charge and isoelectric point of alumina, Mater. Manuf. process. 23 (2008) 615–619.
[30] M. Kosmulski, Compilation of PZC and IEP of sparingly soluble metal oxides and hydroxides from literature, Adv. Colloid Interface Sci. 152 (2009) 14–25.
[31] Q. Xiang, J. Yu, P.K. Wong, Quantitative characterization of hydroxyl radicals produced by various photocatalysts, J. Colloid Interface Sci. 357 (2011) 163–167.
[32] N.C. Halder, C.N.J. Wagner, Separation of particle size and lattice strain in integral breadth measurements, Acta Crystallogr. 20 (1966) 312.
[33] J.C. Medina, M. Bizarro, C.L. Gomez, O. Depablos-Rivera, R. Mirabal-Rojas, B.M. Monroy, A. Fonseca-Garcia, J. Perez-Alvarez, S.E. Rodil, Sputtered bismuth oxide thin films as a potential photocatalytic material, Catal. Today 266 (2016) 144–152.
[34] C.G. Silva, W. Wang, J.L. Faria, Photocatalytic and photochemical degradation of mono-, di- and tri-azo dyes in aqueous solution under UV irradiation, J. Photochem. Photobiol. A Chem. 181 (2006) 314–324.
[35] M.L. Yola, T. Eren, N. Atar, S. Wang, Adsorptive and photocatalytic removal of reactive dyes by silver nanoparticle-colemanite ore waste, Chem. Eng. J. 242 (2014) 333–340.
[36] M.M. Sousa, C. Miguel, I. Rodrigues, A.J. Parola, F. Pina, J.S. Seixas de Melo, M.J. Melo, A photochemical study on the blue dye indigo: from solution to ancient Andean textiles, Photochem. Photobiol. Sci. 7 (2008) 1353–1359.
[37] A.G.S. Prado, L.B. Bolzon, C.P. Pedroso, A.O. Moura, L.L. Costa, Nb2O5 as efficient and recyclable photocatalyst for indigo carmine degradation, Appl. Catal. B Environ. 82 (2008) 219–224.
[38] M.G. Coelho, G.M. de Lima, R. Augusti, D.A. Maria, J.D. Ardisson, New materials for photocatalytic degradation of Indigo Carmine—synthesis, characterization and catalytic experiments of nanometric tin dioxide-based composites, Appl. Catal. B Environ. 96 (2010) 67–71.
[39] M.G. Coelho, F.V. de Andrade, G.M. de Lima, R. Augusti, M.P. Ferreira, D.A. Maria, J.D. Ardisson, Preparation of a new composite by reaction of $SnBu_3Cl$ with $TiCl_4$ in the presence of NH_4O-photocatalytic degradation of indigo carmine, Appl. Organomet. Chem. 25 (2011) 220–225.
[40] T.T. Guaraldo, T.B. Zanoni, S.I.C. de Torresi, V.R. Gonçales, G.J. Zocolo, D.P. Oliveira, M.V.B. Zanoni, On the application of nanostructured electrodes prepared by $Ti/TiO_2/WO_3$ “template”: a case study of removing toxicity of indigo using visible irradiation, Chemosphere 91 (2013) 586–593.
[41] J.C. Medina, M. Bizarro, P. Silva-Bermudez, M. Giorcelli, A. Tagliaferro, S.E. Rodil, Photocatalytic discoloration of methyl orange dye by δ-Bi_2O_3 thin films, Thin Solid Films 612 (2016) 72–81.
[42] F.D. Hardcastle, I.E. Wachs, Determination of niobium oxygen bond distances and bond orders by Raman-spectroscopy, Solid State Ionics 45 (1991) 201–213.
[43] H.F. Zhai, X. Qian, J.Z. Kong, A.D. Li, Y.P. Gong, H. Li, D. Wu, Abnormal phase transition in $BiNbO_4$ powders prepared by a citrate method, J. Alloys Compd. 509 (2011) 10230–10233.
[44] Y.J. Kang, T.H. Ghong, Y.W. Jung, J.S. Byun, S. Kim, Y.D. Kim, T.G. Seong, K.H. Cho, S. Nahm, Optical properties of bismuth niobate thin films studied by spectroscopic ellipsometry, Thin Solid Films 518 (2010) 6526–6530.
[45] A. Hernández-Gordillo, J.C. Medina, M. Bizarro, R. Zanella, B.M. Monroy, S.E. Rodil, Photocatalytic activity of enlarged microrods of α-Bi_2O_3 produced using ethylenediamine-solvent, Ceram. Int. 42 (2016) 11866–11875.
[46] D.E. Sweenor, S.K. O'Leary, B.E. Foutz, On defining the optical gap of an amorphous semiconductor: an empirical calibration for the case of hydrogenated amorphous silicon, Solid State Commun. 110 (1999) 281–286.
[47] Y.N. Guo, L. Chen, F.Y. Ma, S.Q. Zhang, Y.X. Yang, X. Yuan, Y.H. Guo, Efficient degradation of tetrabromobisphenol A by heterostructured $Ag/Bi_5Nb_3O_{15}$ material under the simulated sunlight irradiation, J. Hazard. Mater. 189 (2011) 614–618.
[48] S.M. Zanetti, S.A. da Silva, G.P. Thim, A chemical route for the synthesis of cubic bismuth zinc niobate pyrochlore nanopowders, J. Solid State Chem. 177 (2004) 4546–4551.
[49] L.L. Garza-Tovar, L.M. Torres-Martínez, D.B. Rodríguez, R. Gómez, G. del Angel, Photocatalytic degradation of methylene blue on Bi_2MNbO_7 (M = Al, Fe, In, Sm) sol–gel catalysts, J. Mol. Catal. A Chem. 247 (2006) 283–290.
[50] D.E. Scaife, Oxide semiconductors in photoelectrochemical conversion of solar energy, Sol. Energy 25 (1980) 41–54.
[51] S. Sun, W. Wang, Advanced chemical compositions and nanoarchitectures of bismuth based complex oxides for solar photocatalytic application, RSC Adv. 4 (2014) 47136–47152.